Three-Dimensional Structure of the Nonaheme Cytochrome *c* from *Desulfovibrio desulfuricans* Essex in the Fe(III) State at 1.89 Å Resolution[†,‡]

Stephan Umhau, Günter Fritz,*[,§] Kay Diederichs, Jason Breed, Wolfram Welte,* and Peter M. H. Kroneck

Fachbereich Biologie, Mathematisch-Naturwissenschaftliche Sektion, Universität Konstanz, 78457 Konstanz, Germany

Received June 28, 2000; Revised Manuscript Received November 15, 2000

ABSTRACT: A nine heme group containing cytochrome *c* isolated from the soluble and membrane fractions of *Desulfovibrio desulfuricans* Essex, termed nonaheme cytochrome *c*, was crystallized, and the structure was solved using the multiple wavelength anomalous dispersion (MAD) phasing method. Refinement was carried out to a resolution of 1.89 Å, and anisotropic temperature factors were addressed to the iron and sulfur atoms in the model. The structure revealed two cytochrome c_3 like domains with the typical arrangement of four heme centers. Both domains flanked an extra heme buried under the protein surface. This heme is held in position by loop extensions in each of the two domains. Although both the N- and C-terminal tetraheme domains exhibit a fold and heme arrangement very similar to that of cytochrome c_3, they differ considerably in their loop extensions and electrostatic surface. Analysis of the structure provides evidence for a different function of both domains, namely, anchoring the protein in a transmembranous complex with the N-terminal domain and formation of an electron-transfer complex with hydrogenase by the C-terminal domain.

Sulfate-reducing bacteria utilize inorganic sulfur compounds as terminal electron acceptors, resulting in chemiosmotic energy conservation (*1*). This process is called sulfate respiration and requires eight electrons to reduce sulfate to hydrogen sulfide. The electron-transfer chain of sulfate-reducing bacteria comprises a large variety of *c*-type cytochromes, which had been the subject of intensive investigations. Structural information is available on monoheme cytochrome c_{553} (M_r 9 kDa) (*2*) and a group of multiheme cytochromes such as tetraheme cytochrome c_3 (M_r 14 kDa) (*3*−*11*), octaheme cytochrome c_3, a noncovalently linked dimer of two cytochrome c_3 molecules (M_r 26 kDa) (*12*), and the recently reported nonaheme cytochrome *c* from *Desulfovibrio desulfuricans* ATCC 27774 (M_r 37.5 kDa) (*13*, *14*). The structure of the 16 heme group containing high-molecular-mass cytochrome (referred as HmcA,[1] M_r 67 kDa) (*15*−*18*) has not been analyzed thus far. In the monoheme cytochrome c_{553} the heme iron has methionine−histidine coordination, whereas in the multiheme cytochromes the heme groups are almost bishistidinyl coordinated throughout. The presence of a signal peptide in the primary structure deduced from the nucleotide sequence of all *c*-type cytochromes in *Desulfovibrio* sp. indicates that these proteins are localized in the periplasmic space, where they function as electron carriers. In the periplasmic space of *Desulfovibrio* sp., hydrogen is oxidized by hydrogenase and the electrons are transferred to nonaheme cytochrome *c* and cytochrome c_3 [see following paper (*63*)]. In *Desulfovibrio vulgaris* and *Desulfovibrio gigas* the 16 heme group containing high-molecular-mass cytochrome might act as an additional electron acceptor (*19*). The gene encoding the HmcA protein is part of an operon with six open reading frames encoding a transmembrane electron-transfer complex. This complex is assumed to deliver the electrons from hydrogenase and cytochrome c_3 via HmcA protein to redox proteins at the cytoplasmic site of the membrane, where sulfate reduction occurs. The here described nonaheme cytochrome *c* isolated from *D. desulfuricans* strain Essex (*Dd*E) (*63*) and nonaheme cytochrome *c* from the strain ATCC 27774 (*Dd*A) (*14*) are considered to be functional homologues of the HmcA protein. It was reported that nonaheme cytochrome *c* from *Dd*A and the high-molecular-mass cytochrome *c* from *Dv*H are reduced only very slowly by [Ni,Fe] hydrogenase compared to cytochrome c_3 (*19*). In contrast, nonaheme cytochrome *c* from *Dd*E is reduced at a high rate by [Ni,Fe] hydrogenase, indicating that this cytochrome might act as an additional electron acceptor for hydrogenase in vivo (*63*).

Herein we report the three-dimensional structure of this protein using the multiwavelength anomalous dispersion (MAD) phasing method for structure determination and its refinement to 1.89 Å. The protein folds into two major domains with high structural homology to tetraheme cytochrome c_3 and is connected by a long segment comprising 45 amino acid residues. In the center of the protein an additional heme is coordinated by extensions of the N- and C-terminal domains. Analysis of the folding pattern and electrostatic surface of the protein revealed that both domains most probably have a different function concerning electron transfer and protein−protein interaction.

[†] This work was supported by the Deutsche Forschungsgemeinschaft, Volkswagenstiftung, and Fonds der Chemie (P.M.H.K.).

[‡] Coordinates have been deposited in the RCSB Protein Data Bank (*62*), entry 1DUW.

* To whom correspondence should be addressed. W.W.: tel, +49-7531-882206; fax, +49-7531-883189; e-mail, wolfram.welte@uni-konstanz.de. G.F.: tel, +41-1-635 5554; fax, +41-1-635 5905; e-mail, gfritz@bioc.unizh.ch.

[§] Present address: Biochemisches Institut, Winterthurer Strasse 190, Universität Zürich, CH-8057 Zürich, Switzerland.

[1] Abbreviations: *Dd*A, *Desulfovibrio desulfuricans* ATCC 27774; *Dd*E, *Desulfovibrio desulfuricans* Essex; Hmc, high-molecular-mass cytochrome; MAD, multiple wavelength anomalous dispersion; ncc, nonaheme cytochrome *c*.

10.1021/bi001479a CCC: $20.00
Published on Web 01/09/2001

Table 1: Diffraction Data and Phase Refinement Statistics[a]

	high resolution	peak	point of inflection	remote low	remote high
MAD phasing data					
wavelength (Å)	$\lambda = 0.8345$	$\lambda_1 = 1.7322$	$\lambda_2 = 1.7345$	$\lambda_3 = 1.7450$	$\lambda_4 = 1.070$
resolution (Å)	30−1.89	30−2.6	30−2.6	30−2.6	30−2.6
no. of observations	101894	95089	77753	52379	97154
no. of unique observations	27269	11960	11848	11853	11762
completeness (%)	87.9 (80.6)	99.5 (100)	98.9 (99.6)	98.9 (99.6)	98.4 (99.8)
R_{merge} (%)	7.9 (18.4)	8.4 (17.5)	4.4 (8.4)	5.6 (15.8)	3.3 (6.5)
R_{anom} (%)		7.6 (10.7)	3.4 (5.7)	3.8 (8.8)	3.2 (5.1)
I/σ	9.7 (3.4)	8.8 (4.4)	17.6 (8.4)	14.3 (5.6)	24.0 (12.4)
phasing power statistics					
acentric		0.81	6.08	5.61	
anomalous		4.43	3.12	0.93	1.98
figure of merit (deg)		centric 0.808		acentric 0.718	

[a] $R_{merge} = S|I_{hkl} - \langle I_{hkl}\rangle|/\langle I_{hkl}\rangle$, where I_{hkl} is the intensity of an observation of reflection *hkl* and $\langle I_{hkl}\rangle$ is the average intensity for reflection *hkl*. Values in parentheses denote the highest resolution shell: 1.98−1.89 Å for high-resolution data and 2.7−2.6 Å for the MAD data. Calculated with SHARP (*23*).

MATERIALS AND METHODS

Protein Purification. Nonaheme cytochrome *c* (nc*c*) was obtained from the soluble fraction of *D. desulfuricans* Essex (*63*). The pure protein was concentrated to 8 mg mL^{-1} by ultrafiltration (Amicon, 30 kDa cutoff) and dialyzed against 10 mM Tris-HCl buffer, pH 7.5.

Crystallization and Cryocondition. Crystals of nc*c* were grown by the hanging drop vapor diffusion method. Each drop contained 4 μL of protein solution (8 mg mL^{-1}) and 4 μL of a solution containing 15% (w/v) poly(ethylene glycol) 6000 and 100 mM HEPES/NaOH, pH 7.5; drops were equilibrated against 700 μL of this solution at 18 °C. Crystals grew in the tetragonal space group $P4_12_12$ within 3 weeks to a size of 150 × 150 × 400 μm^3. The unit cell dimensions were refined to $a = b = 55.45$ Å and $c = 236.9$ Å during data processing. There is one molecule per asymmetric unit, corresponding to a Matthews coefficient of 2.44 $Å^3$/Da, and a calculated solvent content of 49% (*20*).

The three-dimensional structure of nc*c* was determined by the MAD method (*21*) using the Fe atoms as anomalous scatters. The data were collected on flash-frozen crystals to minimize radiation damage during exposure to synchrotron radiation. The best cryocondition was the crystallization buffer solution that contained 20% (v/v) glycerol as cryoprotectant; crystals were transferred into the cryoprotectant solution with a capillary. The crystals were equilibrated for 1 min in the cryoprotectant solution and flash frozen in liquid nitrogen. The mosaicity of the crystals did not increase upon freezing compared to the value observed (0.3°) at room temperature.

Data Collection and Processing. For MAD four data sets were measured near the Fe absorption edge from one frozen crystal (100 × 100 × 300 μm^3) on a CCD4 detector system on beamline BW6, DESY, Hamburg. The wavelengths for data collection were adjusted according to an X-ray fluorescence scan, at $\lambda_1 = 1.7322$ Å (peak), $\lambda_2 = 1.7345$ Å (point of inflection), and two remote points at $\lambda_3 = 1.7450$ Å (low) and $\lambda_4 = 1.0700$ Å (high). The high-resolution data set was collected at $\lambda = 0.8345$ Å in two passes from one frozen crystal (150 × 150 × 400 μm^3) at BW7B, DESY, using a MAR Research 345 imaging plate system. In the first pass data were collected to a resolution of 1.89 Å; in the second pass at lower resolution (3.5 Å) the overloads were measured again. All data sets were processed with XDS and scaled with XSCALE (*22*). Data collection and processing statistics are summarized in Table 1.

Structure Determination, Model Building, and Refinement. The nine Fe sites were located with SOLVE (*21*), yielding an overall *z* score value of 43.9 and initial MAD phases. The Fe sites from the SOLVE output were refined with SHARP (*23*), followed by a solvent flattening procedure at 40% with SOLOMON (*24*, *25*). The solvent-flattened electron density map at 2.6 Å was of good quality (overall figure of merit of 0.82). For details of the phase refinement statistics, refer to Table 1. The MAD map was used for model building with the program O (*26*). Initially, the Fe atoms with the nine heme groups were placed; thereafter, the protein model was built. All 289 amino acids were modeled according to the protein sequence (*63*). There was no electron density observed for three amino acid residues at the N-terminus. This model was then refined against the high-resolution data with CNS (*27*). After rigid body refinement the initial values for *R* and R_{free} (*28*) were 46.6% and 50.1%, respectively. For the test set 5% of the reflections were randomly chosen in the 30−1.89 Å resolution range. The standard protocol for simulated annealing at 3500 K, energy minimization, and restrained *B*-factor refinement as implemented in CNS was used for refinement against the full resolution data. The refinement with CNS lead to an *R*-factor of 21.6% ($R_{free} = 23.3\%$) after including water molecules and one glycerol molecule that most probably was bound during cryoprotection. Further refinement was carried out with SHELXL (*29*) on F_o^2 using the same test set of reflections as used in CNS. Additional water molecules were selected in SHELXL. Water molecules with a *B*-factor higher than 70 $Å^2$ were refined at half-occupancy. Taking into account all heme Fe atoms and sulfur atoms of methionine and cysteine residues, anisotropic *B*-factor refinement resulted in a significant drop of the *R*-factor (Table2). Electrostatic surface potentials of cytochrome c_3 and nonaheme cytochrome *c* were calculated using the program MOLMOL (*30*), which implements an algorithm developed by Nicholls and Honig (*31*). Figures 1−3 and 6 were prepared with MOLSCRIPT (*32*) and Raster3D (*33*); Figures 4 and 7 were prepared with DINO (*34*); Figure 8 was generated using MOLMOL (*30*).

Calculation of Electron-Transfer Coupling Factors. Electron-transfer coupling factors between the heme groups in nonaheme cytochrome *c* were calculated using the program

Table 2: Final Refinement Statistics of the High-Resolution Data[a]

resolution limit (Å)	30−1.89
final *R*-factor/R_{free} (%)	18.2/20.4
no. of protein atoms	2188
no. of atoms in nine heme groups	387
fully occupied water molecules	265
half-occupied water molecules	160
ligand	glycerol
anisotropic *B*-factor refinement	9 Fe, 28 S
model rms deviation from ideality	
bond length (Å)	0.01
bond angle (deg)	2.38

[a] The calculations were performed with SHELXPRO (*29*).

HARLEM (*35*) that implements the Pathways model. In the calculations the heme moiety without the propionate and methyl residues was defined as donor or acceptor, respectively.

RESULTS AND DISCUSSION

Overall Structure. There is one molecule in the asymmetric unit cell of the space group $P4_12_12$. This is consistent with the fact that the nonaheme cytochrome *c* from *Dd*E is monomeric. The model consists of 289 amino acid residues and 9 heme groups. No defined electron density is observed for three amino acid residues located at the N-terminus, as determined by Edman sequencing (*63*). Nonaheme cytochrome *c* has an elliptical shape with a length of approximately 80 Å and a diameter of 30 Å.

Very recently, the three-dimensional structure of the nine heme group containing cytochrome *c* from *Dd*A was published, which shows high similarity to the nc*c* from *Dd*E described here (86% sequence identity; rmsd of 288 Cα positions, 0.67 Å). Nc*c* from *Dd*E comprises two cytochrome c_3 like domains with four heme centers, each of which is connected by a long extended segment (Figure 1). This linker region is stabilized by one long and two short α-helices. The stabilizing character is expressed by extensive interactions of α-helices G and H with the N-terminal tetraheme-like domain (Figure 1).

The orientation and arrangement of the hemes within each domain are very similar to those of all tetraheme cytochromes c_3. The polypeptide chain wraps around the porphyrin moieties, which are covalently attached to the protein backbone via two cysteinyl thioether bridges. All nine heme Fe centers are bishistidinyl coordinated (Figure 2). The heme groups are numbered according to their order of bonding to the polypeptide chain through thioether bonds. Hemes I, II, III, and V are accommodated by the N-terminal domain and hemes VI−IX by the C-terminal domain. Heme IV is located between these two domains (Figures 1 and 3). Although all heme groups share the same structural features, heme IV appears to be exceptional. Whereas the eight heme groups of the cytochrome c_3 like domains are accessible to the solvent, heme IV is completely buried within the protein (Figure 4). Furthermore, the coordination pattern of heme IV is unique compared to the other heme groups in the molecule. The two residues, Cys111 and Cys114, which form the thioether bonds, and His115, which coordinates the iron of heme IV, are located on an extension of a loop in the N-terminal domain that is inserted into the cytochrome c_3 like structure. His218, which completes the octahedral coordination of the iron center, is located on an extension of a loop in the C-terminal domain. This structural arrangement emphasizes the role of heme IV as a bridging element between the N- and C-terminal domains of nc*c*.

Arrangements of Hemes. The location of the nine hemes including the distances between the individual iron centers is depicted in Figure 3. The position and the distances of the heme groups in the N- and C-terminal domain of nc*c* are almost identical to those in cytochrome c_3 (Table3).

Heme IV is located between the tetraheme clusters. According to the Fe−Fe distances the central heme group is located closer to the N-terminal heme cluster (heme IV−III distance, 13.3 Å) than to the C-terminal cluster (heme IV−VI, 16.3 Å; heme IV−VIII, 16.6 Å). However, with regard to the porphyrin edge-to-edge distances heme IV is positioned almost perfectly in the center of the two domains (N-terminal domain, hemes III−IV, 8.4 Å; C-terminal domain, hemes VIII−IV, 8.7 Å). Another striking feature is the linear and perfect coplanar arrangement of hemes V (N-terminal domain), IV (central heme), and VIII (C-terminal domain) with porphyrin edge-to-edge distances of 10.0 Å between hemes V and IV and 8.7 Å between hemes IV and VIII. Such an alignment of aromatic redox cofactors has been observed previously in electron-transfer complexes (*36*−*40*). It allows maximum overlap between the π-electron of the individual porphyrin ring systems, thus facilitating electron transfer. It is concluded that heme IV operates as an electron-conducting element between the N- and C-terminal tetraheme building blocks. Most likely, nonaheme cytochrome *c* was formed by gene duplication of the gene encoding tetraheme cytochrome c_3. However, it appears that nc*c* is not just a simple duplicate of cytochrome c_3 but more likely represents a novel kind of multiheme protein with slightly different structural features using the basic architecture of cytochrome c_3. Variations of the basic cytochrome c_3 structure in the N- and C-terminal domains of nonaheme cytochrome *c* were analyzed by comparison of the secondary structure topology of the two proteins.

Topological Comparison of the Nonaheme Cytochrome c with the Tetraheme Cytochrome c_3. To get a deeper insight, the secondary structure topology of nc*c* and cytochrome c_3 of *Dd*E was compared (Figure 5). Although the sequence similarity between the N- and C-terminal domains of nc*c* and cytochrome c_3 is similarly low (36% and 34% similarity, respectively), the two domains resemble the c_3 molecule in a different way. Consistent with the apparent conservation of the heme arrangement in the N- and C-terminal domains of both proteins, the key structural features at the heme sites are almost identical. This includes the short antiparallel β-sheets followed by two short α-helices (A, B), a long loop (loop 3) of approximately 30 amino acids, and a long α-helix that is interrupted by a loop (helices C and D, loop 4).

Obviously, the N-terminal domain of nc*c*, in comparison to its C-terminal domain, resembles more closely cytochrome c_3. In comparison to cytochrome c_3 the N-terminal helix A is extended, and the following loop 2 is therefore slightly shortened (Figure 5). Heme center IV is accommodated by helix E, which is absent in cytochrome c_3. Furthermore, loop 1 and loop 4 are elongated in comparison to the corresponding loops in cytochrome c_3 (Figures 5 and 6).

The topological homology between cytochrome c_3 and the C-terminal domain of nc*c* is less evident. Helix J corresponds to helix A in cytochrome c_3 but is almost three times longer. It forms a basis for the following loop−helix K−loop

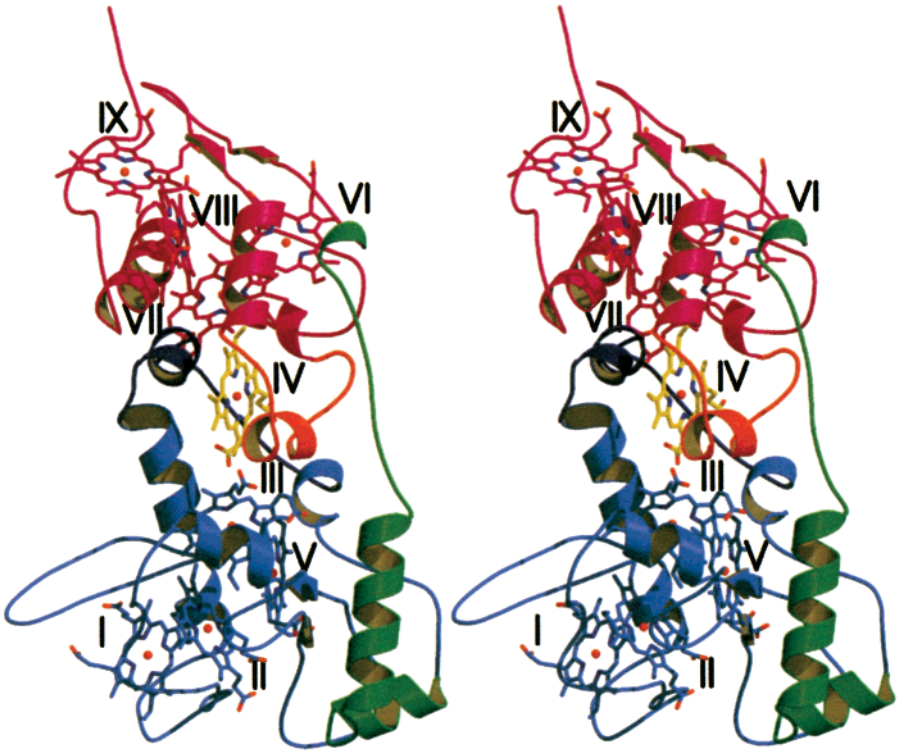

FIGURE 1: Stereo representation of the structure of nonaheme cytochrome *c*. The N- and C-terminal domains are colored in blue and magenta, respectively. The covalent connection of both domains by an elongated loop and one long and two short α-helices is shown in green. The heme groups are shown in ball-and-stick type; the central heme group IV between the domains is shown in yellow. The extensions of the N- and C-terminal domains that coordinate heme IV are illustrated by brighter colors. Figures 1, 2, 3, and 6 were produced with MOLSCRIPT (*32*) and Raster3D (*33*).

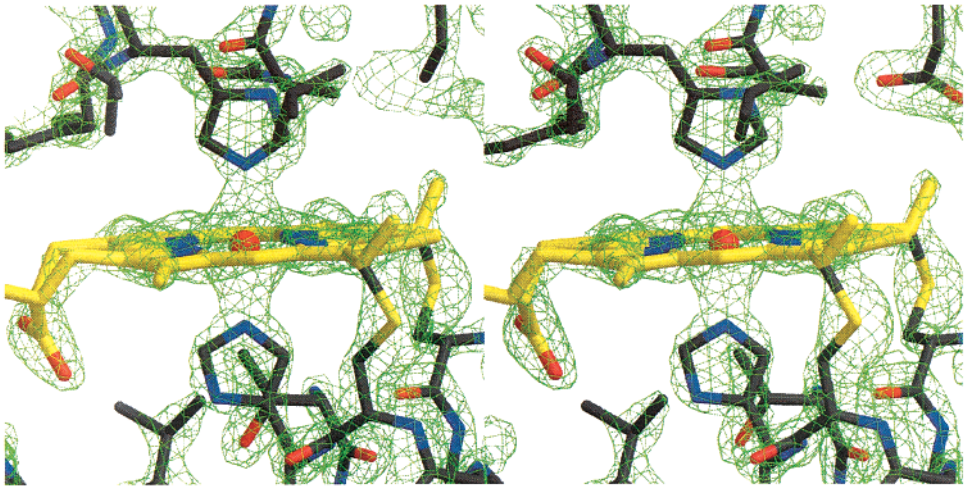

FIGURE 2: Stereo representation of the attachment and coordination of heme IV. The models of the porphyrin (yellow) and the interacting amino acid residues (gray) are superimposed with the corresponding electron density map (green). The $2F_o - F_c$ map is shown at 3δ.

structure that is necessary for coordination of heme IV. Surprisingly, loop 4, which is present both in the N-terminal domain of nc*c* and in cytochrome c_3, is missing in the C-terminal domain of nc*c*, fusing helices C and D from cytochrome c_3 to form helix M in nc*c*. The long segment between the N- and C-terminal domains, which includes helices G, H, I, and a long loop, does not show any topological homology to cytochrome c_3.

The superposition of the two domains in nc*c* (Figure 6) illustrates the consequences of insertions and deletions. The Cα positions of the N-terminal (residues 10−132) and the C-terminal domains (residues 177−287) and cytochrome c_3 (107 residues) were aligned by employing a six-dimensional search algorithm (*41*, *42*). The core structural elements (36 Cα positions) of the tetraheme-like domains are well conserved and could be superimposed with a rmsd of 1.4 Å; the overlay of the two domains with cytochrome c_3 gave the same value. In contrast, major differences were observed in the length of several loops. Each domain exhibits an extended loop comprising short α-helical segments, which supply the coordination for heme IV (Figure 6). Additional differences between cytochrome c_3 and the two domains of nc*c* were localized in the loop regions of the proteins. Loop 1 connecting the antiparallel β-sheets is elongated in both domains of nc*c*. In cytochrome c_3, this loop consists of four residues. In the C-terminal domain of nc*c*, the corresponding

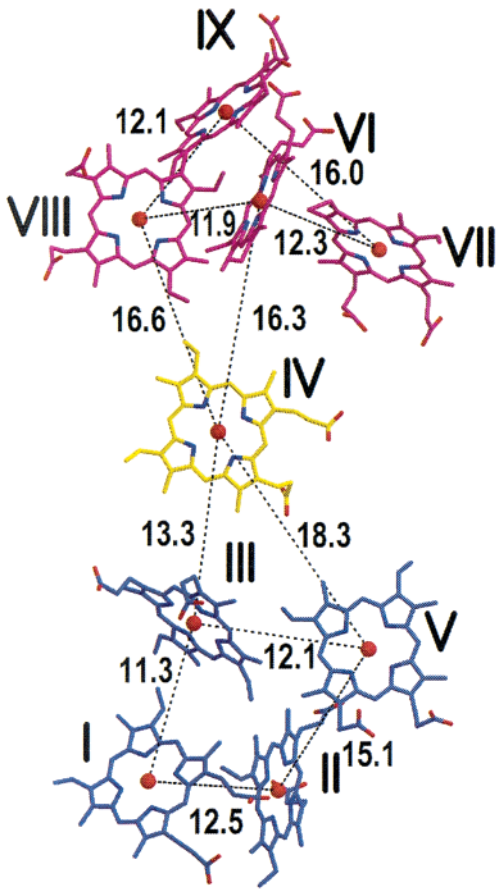

FIGURE 3: Orientation of the heme groups in nonaheme cytochrome *c*. The heme groups are numbered according to their covalent attachment through cysteine residues to the protein. The heme groups of the N-terminal tetraheme cluster are depicted in blue, the heme groups of the C-terminal domain are in magenta, and the central heme IV is in yellow. Iron−iron distances are given in angstroms.

loop is built of 9 amino acid residues, and in the N-terminal domain 16 residues form a large loop. Further variations occur in loop 4 that is interrupting the long central helix in cytochrome c_3, resulting in helices C and D. In cytochrome c_3 the loop comprises 9 residues. In the N-terminal domain of nc*c* the corresponding loop has 15 residues, whereas it is absent in the C-terminal domain. Note that these loops are located at the surface of the molecules. In cytochrome c_3 loops 1 and 4 form rather inconspicuous patches at the protein surface whereas in the N-terminal domain of nc*c* these loops represent remarkable features, which are asymmetrically distributed in nc*c*. Whereas the long loops in the N-terminal domain are standing out of the surface (Figure 7), loop 1 of the C-terminal domain is embedded into the surface of nc*c*. This remarkable difference between the two domains suggests that they might have different functions. The bulbs formed by loops 1 and 4 in the N-terminal domain might be important for anchoring nc*c* into the Hmc complex, whereas the C-terminal domain accepts electrons from the electron donor. Further arguments for this hypothesis will be derived from the analysis of the electrostatic potential of nc*c*.

Electrostatic Surface Potential. Generally, intermolecular electron transfer between redox proteins requires the formation of a transient complex, followed by the fast transfer of electrons. The complex formation is mainly driven by Coulombic interaction via electric charges on the protein surfaces (*38*, *43*−*45*). In cytochrome c_3, heme IV is surrounded by a large cloud of positively charged residues (Figure 8B). The other hemes, in contrast, are surrounded by residues forming both negative and positive charges. In numerous studies on intermolecular electron transfer it was shown that the interaction of the tetraheme cytochrome c_3 with redox partners such as ferredoxin (*46*−*52*), flavodoxin (*38*−*40*, *53*−*56*), and rubredoxin (*39*, *53*) was mediated by ion pair formation between this positively charged patch on cytochrome c_3 and negative charges of the partner molecule. The crystal structure of the [Ni,Fe] hydrogenase from *D. gigas* revealed a negatively charged surface area formed by acidic residues around the histidine coordinating the distal [4Fe-4S] center that is thought to transfer the electrons liberated in hydrogen oxidation (*57*).

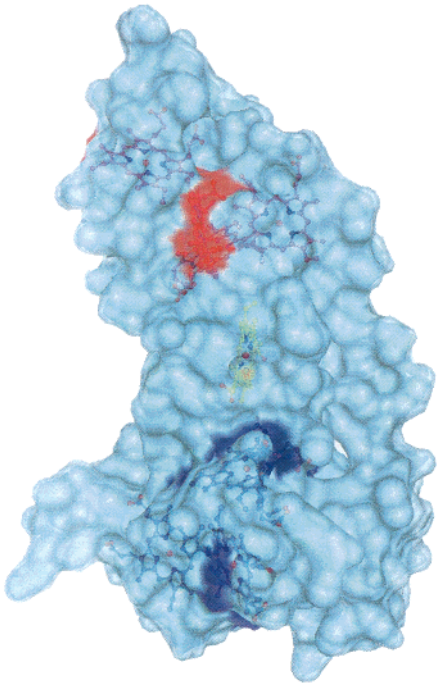

FIGURE 4: Surface representation of nonaheme cytochrome *c*. Colored areas indicate the accessibility of the heme groups. The N-terminal tetraheme cluster is shown in blue and the C-terminal in red. The central heme IV is almost completely buried in the protein. Figures 4 and 7 were prepared with DINO (*34*).

Since both cytochrome c_3 and nc*c* coupled to the [Ni,Fe] hydrogenase from *Dd*E with similar affinity and exhibited similar reaction rates in the presence of dihydrogen (*63*), the environment of the heme groups in nc*c* was examined with respect to surface charge distribution, which clearly differed in the two domains. On the N-terminal domain there are no positive patches around the surface-exposed hemes, which would allow electrostatic interaction with a negatively charged reaction partner. In contrast, heme VIII in the C-terminal domain is surrounded by lysine (positions 180, 209, 212, 280) and arginine residues (positions 108, 109, 198, 199, 207, 278). This region forms a large positively charged plane at the surface (Figure 8A) that can be accessed by a rather large molecule such as the [Ni,Fe] hydrogenase. On the basis of these considerations it is proposed that heme center VIII of nc*c* functions as the electron acceptor for [Ni,-

Table 3: Fe−Fe Distances in the Nonaheme Cytochrome *c* from *D. desulfuricans* Essex[a]

	heme I	(VI)	heme II	(VII)	heme III	(VIII)	heme V	(IX)
heme I (VI)								
heme II (VII)	12.5	(12.3)						
heme III (VIII)	11.3	(11.9)	15.8	(16.6)				
heme V (IX)	17.7	(17.4)	15.1	(16.0)	12.1	(12.1)		
heme IV	24.5	16.3	26.3	17.7	13.3	16.6	18.3	25.8

[a] The Fe−Fe distances between heme groups I, II, III, and V in the N-terminal domain and between heme groups VI, VII, VIII, and IX in the C-terminal domain (in parentheses) are given; furthermore, the distances from the Fe of heme IV to the Fe in the residual heme centers are listed. To compare the distances in each tetraheme cluster of the N- and C-terminal domains, the corresponding Fe−Fe distances are listed next to each other.

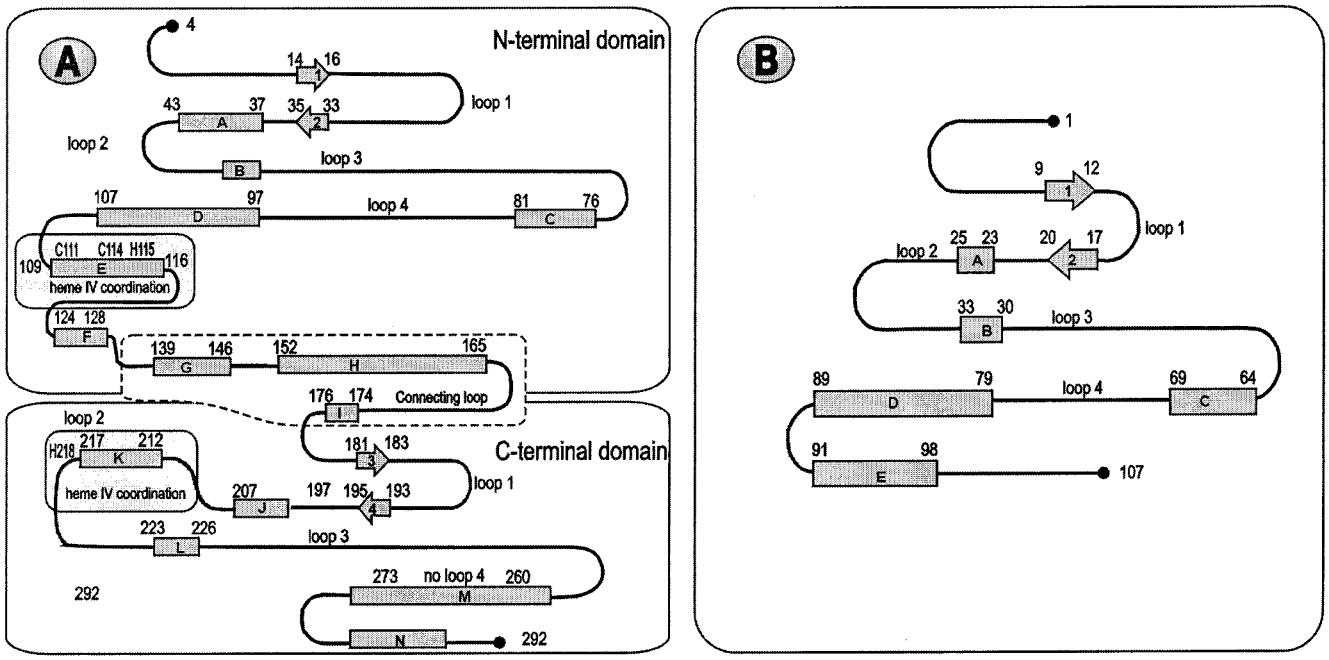

FIGURE 5: Topology diagrams of nonaheme cytochrome *c* and cytochrome c_3. The secondary structure topology of nonaheme cytochrome *c* (A) and cytochrome c_3 (B) is compared. Lines represent loop regions, arrows correspond to β-strands, and α-helices are depicted as rectangles. The regions which interact with the central heme IV (A) are highlighted by shadowed boxes. A broken line encloses the segment that connects the N- and C-terminal domains.

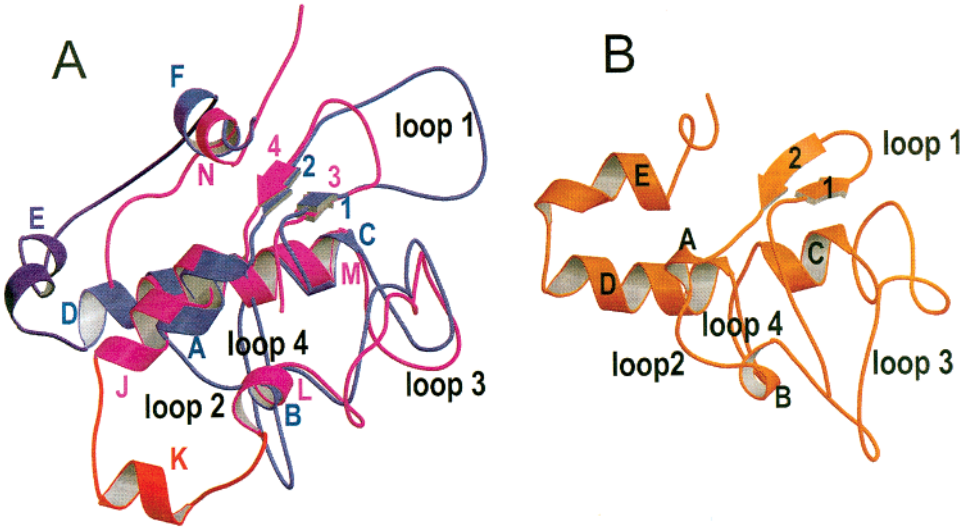

FIGURE 6: Structural alignment of the N-terminal (magenta) and C-terminal (blue) domains of nonaheme cytochrome *c* (A) with cytochrome c_3 (B). For reasons of clarity the domains of nonaheme cytochrome *c* are superimposed, and cytochrome c_3 is shown in the same orientation.

Fe] hydrogenase. Interestingly, heme VIII in the homologous ncc from *Dd*A is encircled by a large number of lysine and arginine residues, too (*13*, *14*). However, the calculated electrostatic surface potential in this region appears to be less positive. This might be due to an additional aspartatic acid residue (position 210) and one exchange of an arginine to a serine residue (position 207) compared to the ncc from *Dd*E.

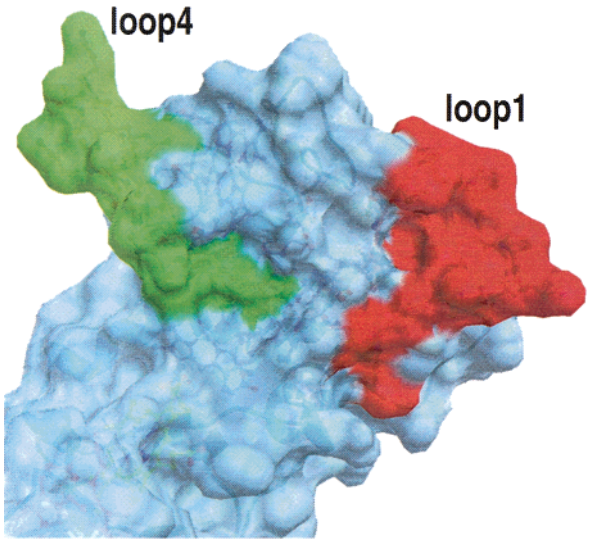

FIGURE 7: Surface representation of the N-terminal domain of nonaheme cytochrome *c*. The residues forming loops 1 and 4 are colored in red and green, respectively. These loops are elongated compared to the C-terminal domain of ncc or cytochrome c_3 and form extensions that might anchor nonaheme cytochrome *c* in the Hmc complex.

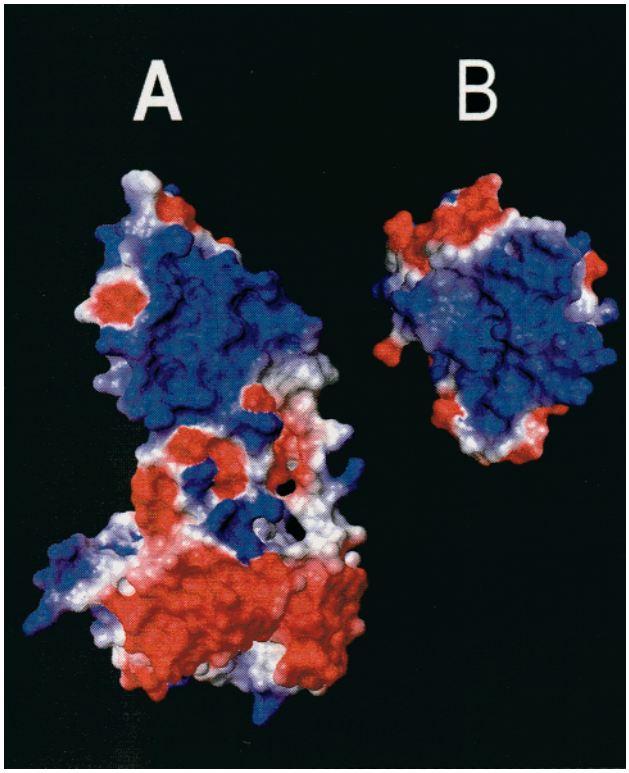

FIGURE 8: Electrostatic surface potential of nonaheme cytochrome *c* and cytochrome c_3. The electrostatic charge distribution of nonaheme cytochrome *c* (A) and cytochrome c_3 (B) was calculated using MOLMOL (*30*). Both molecules are shown at the same scale. Positive and negative charges are depicted in blue and red, respectively. The positively charged areas around heme VIII in ncc and around heme IV in cytochrome c_3 are proposed to act as the coupling site to [Ni,Fe] hydrogenase. The figure was produced with MOLMOL.

Electron Transfer. Most electron-transfer reactions in biology occur over a considerable distance (>5 Å) whereby the electron is shifted via electron tunneling. The electron-transfer rates are nonadiabatic and can be expressed as

$$k_{ET} = (2\pi/\hbar)T_{DA}^{2}(FC)$$

(*58*). The transfer rate is dependent on the coupling between the donor and the acceptor, represented as the term T_{DA}, and the Gibbs free energy and the reorganization energy, which are contained in the term *FC*, the so-called Franck−Condon factor. In the Pathways model (*59*, *60*) the electron tunneling pathway between the donor and acceptor is divided into through-bond (covalent and hydrogen bonds) and through-space (van der Waals contacts) interactions. These are reflected in different coupling factors. The most favorable pathway will be the one with the smallest coupling decay, i.e., with the largest coupling factor.

The electron-transfer properties of nonaheme cytochrome *c* were studied using the program HARLEM developed by Kurnikov (*35*). Two characteristics of electron transfer were analyzed. First, the intramolecular transfer properties are characterized by the electronic coupling factors between the heme groups in nonaheme cytochrome *c*. The calculated coupling factors (Figure 9) were similar to those determined for nonaheme cytochrome *c* from *Dd*A (*13*). The observed differences are most likely due to the fact that the authors used the program GREENPATH (*61*). In this program several changes were introduced with regard to Pathways calculations (*60*), whereas HARLEM (*35*) implements the original Pathways algorithm (I. Kurnikov, personal communication). However, the coupling values between the parallel oriented heme groups V, IV, and VIII were not taken into account, although these coupling factors are in the range of those observed for the hemes in each tetraheme cluster of ncc. In particular, the coupling between heme VIII and heme IV is considerable high. This observation fits our conclusions from electrostatic surface potential calculations that heme VIII most likely acts as the electron entry for electrons from the [Ni,Fe] hydrogenase. Furthermore, it emphasizes the role of heme IV as a conducting element between the N- and C-terminal tetraheme clusters.

Second, a possible site for intermolecular electron transfer between nonaheme cytochrome *c* and [Ni,Fe] hydrogenase was mapped on the surface of the protein by calculating the electronic coupling factors between each heme group and any residue of the protein. Regions on the surface with high coupling values have a large probability for electron transfer. In general, the C-terminal domain displayed more areas with high coupling values than the N-terminal domain (Figure 9). Surface patches with high coupling values were observed around hemes VII and VIII. The region around heme VII was not accessible by large redox partners such as hydrogenase. In contrast, the patch around heme VIII displaying high electron coupling values was located in a planar region of the protein's surface, facilitating intermolecular contacts. The driving force for an association of [Ni,Fe] hydrogenase to this region of nonaheme cytochrome *c* is given by Coulombic interaction. As shown above (Figure 8A) this region is highly positively charged and could form a complex with the negatively charged area around the distal [4Fe-4S] cluster of [Ni,Fe] hydrogenase. Therefore, we conclude that the electrons from the [Ni,Fe] hydrogenase enter nonaheme cytochrome *c* at heme VIII. From there the electrons can be transferred very fast to hemes VI, IX, and IV as indicated by high coupling values between heme VIII and these heme groups.

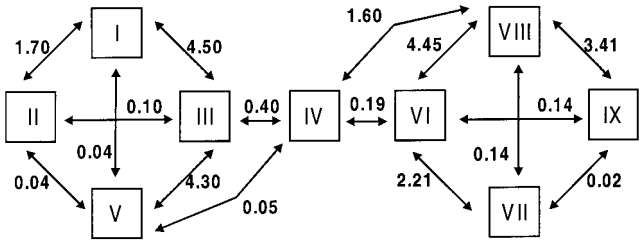

FIGURE 9: Intramolecular electron transfer of nonaheme cytochrome *c*. The numbers represent the relative electron-transfer coupling factors between the heme groups multiplied by 1000. The numbers are calculated by the Pathways model and are dimensionless.

Redox-Induced Conformational Transition. Reduction of the Fe(III) heme centers of nc*c* led to significant changes of the surface charge and of the protein conformation (*63*): (i) the hydrodynamic radius of dithionite-reduced nc*c* increased according to size exclusion chromatography; (ii) this conformational transition was confirmed by CD spectroscopy; (iii) further evidence was obtained from p*I* determinations of the oxidized and reduced protein revealing a large drop of p*I* upon reduction; (iv) addition of sodium dithionite to crystalline Fe(III) nc*c*, in the absence of dioxygen, produced a clearly visible color change from red to magenta. Within a few seconds, the magenta crystals started to crack and the protein became finally dissolved. The results of these four independent observations led to the hypothesis of a redox-dependent conformational transition of nc*c* due to a potential hinge in the center of the molecule. Most likely, this conformational change should occur in the linker region between the two rigid tetraheme cytochrome c_3 like domains. These are covalently linked by an elongated segment with temperature factors significantly higher than the average *B*-factor of the entire peptide chain, which argues for its flexibility. The rigid coordination of heme IV is most probably not affected by the movement. A hinge might be formed by the short α-helices in the extended loops coordinating heme IV and helices from each domain which are in van der Waals contact. This mainly hydrophobic contact is flexible compared to polar or ionic interactions and might allow a gliding movement. The trigger for such a conformational change might originate from the protonation of a heme propionate group and subsequent loss of salt bridges to lysine or arginine residues. The positively charged groups of these residues would be exposed to Coulombic repulsion and might form new salt bridges, stabilizing another conformation. Such a movement within the protein would explain the biochemical data.

Currently, we are analyzing the structure of Fe(II) nc*c* to get further insight into the nature of these reduction-induced conformational changes.

CONCLUSIONS

The three-dimensional structure of nonaheme cytochrome *c* from *D. desulfuricans* Essex represents a combination of the well-known structural features of cytochrome c_3 and new structural aspects. There are two cytochrome c_3 like domains and one extra heme (heme IV) on the interface between the two domains. The way this additional heme center is coordinated in the center of the protein has not been observed before in other than nonaheme cytochrome *c* multiheme redox proteins. The cysteine residues for covalent attachment of the porphyrin and one coordinating histidine are located on one domain. The octahedral coordination of the heme iron is completed by a second histidine located on the other domain. The position of the heme between the two domains and its coordination by histidine residues from both domains illustrate its function as an interdomain electron-transfer bridge. This was affirmed by the electron coupling factors between heme IV and the heme groups from both domains.

It was shown by kinetic studies that the [Ni, Fe] hydrogenase couples at high rate and with high affinity to nonaheme cytochrome *c* (*63*). On the basis of electrostatic and electron coupling calculations, we identified a site in the C-terminal domain that most likely serves as the coupling site to the [Ni,Fe] hydrogenase. This site is positively charged, enabling docking to the negatively charged electron exit site of the [Ni,Fe] hydrogenase. The high coupling factors in this area indicate a high probability of electron transfer upon docking. In the center of this area heme VIII is located. This heme group exhibits the highest coupling factors to the other heme groups in nc*c*, including the central bridging heme IV.

Detailed comparison of both domains of nc*c* with cytochrome c_3 revealed that the variation of the cytochrome c_3 basic structure might reflect a specialization in function. Whereas the C-terminal domain represents an optimized electron entry, the N-terminal domain might anchor the molecule in the membrane-bound Hmc complex.

ACKNOWLEDGMENT

Thanks are expressed to Oliver Einsle and Albrecht Messerschmidt for the structural data of cytochrome c_3 from *D. desulfuricans* Essex prior to publication and to Gleb P. Bourenkov and Hans D. Bartunik for help on the BW6 beamline at DESY in Hamburg.

REFERENCES

1. LeGall, J., and Fauque, G. (1988) in *Biology of anaerobic microorganisms* (Zehnder, A. J. B., Ed.) pp 587−639, John Wiley and Sons, New York.
2. Blackledge, M. J., Medvedeva, S., Ooncin, M., Guerlesquin, F., Bruschi, M., and Marion, D. (1995) *J. Mol. Biol. 245*, 661−681.
3. Haser, R., Pierrot, M., Frey, M., Payan, F., Astier, J. P., Bruschi, M., and Le Gall, J. (1979) *Nature 282*, 806−810.
4. Pierrot, M., Haser, R., Frey, M., Payan, F., and Astier, J. P. (1982) *J. Biol. Chem. 257*, 14341−14348.
5. Higuchi, Y., Kusunoki, M., Matsuura, Y., Yasuoka, N., and Kakudo, M. (1984) *J. Mol. Biol. 172*, 109−139.
6. Matias, P. M., Frazão, C., Morais, J., Coll, M., and Carrondo, M. A. (1993) *J. Mol. Biol. 234*, 680−699.
7. Czjzek, M., Payan, F., Guerlesquin, F., Bruschi, M., and Haser, R. (1994) *J. Mol. Biol. 243*, 653−667.
8. Morais, J., Palma, P. N., Frazão, C., Caldeira, J., LeGall, J., Moura, I., Moura, J. J., and Carrondo, M. A. (1995) *Biochemistry 34*, 12830−12841.
9. Matias, P. M., Morais, J., Coelho, R., Carrondo, M. A., Wilson, K., Dauter, Z., and Sieker, L. (1996) *Protein Sci. 5*, 1342−1354.
10. Nørager, S., Legrand, P., Pieulle, L., Hatchikian, C., and Roth, M. (1999) *J. Mol. Biol. 290*, 881−902.
11. Brennan, L., Turner, D. L., Messias, A. C., Teodoro, M. L., LeGall, J., Santos, H., and Xavier, A. V. (2000) *J. Mol. Biol. 298*, 61−82.
12. Czjzek, M., Guerlesquin, F., Bruschi, M., and Haser, R. (1996) *Structure 4*, 395−404.

13. Matias, P. M., Saraiva, L. M., Soares, C. M., Coelho, A., V., LeGall, J., and Carrondo, M. A. (1999) *JBIC, J. Biol. Inorg. Chem. 4*, 478−494.
14. Matias, P., Coelho, R., Pereira, I. A. C., Coelho, A. V., Thompson, A. W., Sieker, L. C., LeGall, J., and Carrondo, M. A. (1999) *Structure 7*, 119−130.
15. Bruschi, M., Bertrand, P., More, C., Leroy, G., Bonicel, J., Haladjian, J., Chottard, G., Pollock, W. B., and Voordouw, G. (1992) *Biochemistry 31*, 3281−3288.
16. Rossi, M., Pollock, W. B. R., Reij, M. W., Keon, R. G., Fu, R., and Voordouw, G. (1993) *J. Bacteriol. 175*, 4699−4711.
17. Verhagen, M. F., Pierik, A. J., Wolbert, R. B., Mallee, L. F., Voorhorst, W. G., and Hagen, W. R. (1994) *Eur. J. Biochem. 225*, 311−319.
18. Pereira, I. A. C., Romão, C. V., LeGall, J., Xavier, A. V., and Teixeira, M. (1997) *J. Bioinorg. Chem. 2*, 23−31.
19. Pereira, I. A. C., Romão, C. V., Xavier, A. V., LeGall, J., and Teixeira, M. (1998) *JBIC, J. Biol. Inorg. Chem. 3*, 494−498.
20. Matthews, B. W. (1968) *J. Mol. Biol. 33*, 491−497.
21. Terwilliger, T., and Berendzen, J. (1997) *Acta Crystallogr., Sect. D 53*, 571−779.
22. Kabsch, W. (1988) *J. Appl. Crystallogr. 21*, 916−924.
23. De LaFortelle, E., and Bricogne, G. (1997) *Methods Enzymol. 276*, 472−494.
24. Abrahams, J. P., and Leslie, A. G. W. (1996) *Acta Crystallogr., Sect. D 52*, 30−42.
25. CCP4 (1994) *Acta Crystallogr., Sect. D 50*, 760−763.
26. Jones, T. A., Zou, J. Y., Cowan, S. W., and Kjeldgaard, M. (1991) *Acta Crystallogr., Sect. A 47*, 110−119.
27. Brünger, A. T., Adams, P. D., Clore, G. M., DeLano, W. l., Gros, P., Grosse-Kunstleve, R. W., Jiang, J.-S., Kuszewski, J., Nilges, M., Pannu, N. S., Read, R. J., Rice, L. M., Simson, T., and Warren, G. L. (1998) *Acta Crystallogr., Sect. D 53*, 905−921.
28. Brünger, A. T. (1992) *Nature 355*, 472−475.
29. Sheldrick, G. M., and Schneider, T. R. (1997) *Methods Enzymol. 277*, 319−343.
30. Koradi, R., Billeter, M., and Wüthrich, K. (1996) *J. Mol. Graph*ics *14*, 51−55.
31. Nicholls, A., and Honig, B. (1990) *J. Comput. Chem. 12*, 435−445.
32. Kraulis, P. J. (1991) *J. Appl. Crystallogr. 24*, 946−950.
33. Merrit, E. A., and Bacon, D. J. (1997) *Methods Enzymol. 277*, 505−524.
34. DINO: Visualizing Structural Biology (2000) http://www-.bioz.unibas.ch/∼xray/dino.
35. Kurnikov, I. V. (2000) HARLEM molecular modeling package, v1.0, Department of Chemistry, University of Pittsburgh, Pittsburgh, PA.
36. Poulos, T. L., and Kraut, J. (1980) *J. Biol. Chem. 255*, 10322−10330.
37. Poulos, T. L., and Mauk, A. G. (1983) *J. Biol. Chem. 258*, 7369−7373.
38. Stewart, D. E., LeGall, J., Moura, J. J. G., Peck, H. D., Jr., Xavier, A. V., Weiner, P. K., and Wampler, J. E. (1988) *Biochemistry 27*, 2444−2450.
39. Stewart, D. E., and Wampler, J. E. (1991) *Proteins 11*, 142−152.
40. Palma, P. N., Moura, I., LeGall, J., Beeumen, J. V., Wampler, J. E., and Moura, J. J. G. (1994) *Biochemistry 33*, 6394−6407.
41. Diederichs, K. (1995) *Proteins 23*, 187−195.
42. Lu, G. (1998) http://bioinfo1.mbfys.lu.se/TOP/maps.html.
43. Chen, L., Durley, R., Mathews, F., and Davidson, V. (1994) *Science 264*, 86−90.
44. Davidson, V. (2000) *Acc. Chem. Res. 33*, 87−93.
45. Zhu, Z., Cunane, L., Chen, Z., Durley, R., Mathews, F., and Davidson, V. (1998) *Biochemistry 37*, 17128−17136.
46. Guerlesquin, F., Bruschi, M., and Bovier-Lapierre, G. (1984) *Biochimie 66*, 93−99.
47. Guerlesquin, F., Noailly, M., and Bruschi, M. (1985) *Biochem. Biophys. Res. Commun. 130*, 1102−1108.
48. Guerlesquin, F., Sari, J. C., and Bruschi, M. (1987) *Biochemistry 26*, 7438−7443.
49. Cambillau, C., Frey, M., Mosse, J., Guerlesquin, F., and Bruschi, M. (1988) *Proteins 4*, 63−70.
50. Dolla, A., Guerlesquin, F., Bruschi, M., and Haser, R. (1991) *J. Mol. Recognit. 4*, 27−33.
51. Park, J. S., Kano, K., Morimoto, Y., Higuchi, Y., Yasuoka, N., Ogata, M., Niki, K., and Akutsu, H. (1991) *J. Biomol. NMR 1*, 271−282.
52. Dolla, A., Leroy, G., Guerlesquin, F., and Bruschi, M. (1991) *Biochim. Biophys. Acta 1058*, 171−177.
53. Stewart, D. E., LeGall, J., Moura, I., Moura, J. J. G., Peck, H. D., Jr., Xavier, A. V., Weiner, P. K., and Wampler, J. E. (1989) *Eur. J. Biochem. 185*, 695−700.
54. DeFrancesco, R., Edmondson, D. E., Moura, I., Moura, J. J. G., and LeGall, J. (1994) *Biochemistry 33*, 10386−10392.
55. Feng, Y., and Swenson, R. P. (1997) *Biochemistry 36*, 13617−13628.
56. Correia, C., Monzani, E., Moura, I., Lampreia, J., and Moura, J. J. (1999) *Biochem. Biophys. Res. Commun. 256*, 367−371.
57. Volbeda, A., Charon, M. H., Piras, C., Hatchikian, E. C., Frey, M., and Fontecilla-Camps, J. C. (1995) *Nature 373*, 580−587.
58. Marcus, R. A. (1956) *J. Chem. Phys. 24*, 966−978.
59. Beratan, D. N., Onuchic, J. N., Winkler, J. R., and Gray, H. B. (1992) *Science 258*, 1740−1741.
60. Onuchic, J. N., Beratan, D. N., Winkler, J. R., and Gray, H. B. (1992) *Annu. Rev. Biophys. Biomol. Struct. 21*, 349−377.
61. Regan, J. J. (1994) Greenpath Software v. 0.971, San Diego, CA.
62. Berman, H. M., Westbrook, J., Feng, Z., Gilliland, G., Bhat, T. N., Weissig, H., Shindyalov, I. N., and Bourne, P. E. (2000) *Nucleic Acids Res. 28*, 235−242.
63. Fritz, G., Griesshaber, D., Seth, O., and Kroneck, P. M. H. (2001) *Biochemistry 40*, 1317−1324.

BI001479A